Journal of Microscopy, Vol. 198, Pt 3, June 2000, pp. 162–173.
Received 26 July 1999; accepted 31 January 2000

Measurement of glutathione levels in intact roots of *Arabidopsis*

M. D. FRICKER*, M. MAY†, A. J. MEYER*, N. SHEARD* & N. S. WHITE*
**Department of Plant Sciences, University of Oxford, South Parks Road, Oxford, OX1 3RB, U.K.*
†Plant Genetic Systems NV, Jozef Plateaustraat 22, B-9000 Gent, Belgium

Key words. *Arabidopsis thaliana*, confocal laser scanning microscopy, fluorescence attenuation correction, glutathione, glutathione S-transferase, monochlorobimane, roots.

Summary

Levels of glutathione were measured for different cell types in roots of intact *Arabidopsis* seedlings after labelling with monochlorobimane to give fluorescent glutathione S-bimane (GSB) and imaging using confocal laser scanning microscopy with excitation at 442 nm. Labelling increased to a plateau in most cell types after about 15–20 min and the GSB accumulated rapidly in the vacuole. Formation of GSB in the cytoplasm was not affected by treatment with sodium azide; however, vacuolar transport of GSB was substantially inhibited under these conditions. We infer that vacuolar sequestration was mediated by a tonoplast glutathione S-conjugate pump. Quantitative estimates of the cytoplasmic glutathione concentration involved correction for the loss in fluorescence signal with depth into the specimen using an empirically determined model derived *in situ* from a permeabilized root. Correction for the dilution experienced on transport into the vacuole also required an estimate of the amount of cytoplasm present in each cell type. This was achieved in two stages: first, the levels of protein were mapped after fixation, permeabilization and labelling with fluroescein isothiocyanate. Second, the corresponding cytoplasmic volume was determined as 40% for epidermal cells in the elongation zone by manual segmentation of the cytoplasm in serial optical sections. Values of relative cytoplasmic volume for other cells were extrapolated in proportion to their protein content. Using this approach, cytoplasmic glutathione concentrations were found to be 2–3 mM in most cell types. There was a marked difference between the central cells and the neighbouring, rapidly dividing initials, and between the columella cells and the outermost cells of the root cap. In the latter case, the difference was equalized in the presence of azide. This might indicate that additional cell–cell movement and preferential sequestration of GSB can occur during the detoxification process in an intact system.

Correspondence to: Dr M. D. Fricker. Fax: + 44 (0)1865 275074; e-mail: mark.fricker@plant-sciences.ox.ac.uk

Introduction

The tripeptide glutathione (GSH: γ-glutamyl-cysteinyl-glycine) is the most abundant low molecular weight thiol in plants and participates in a wide range of different metabolic pathways, including DNA synthesis, detoxification of electrophiles, vacuolar sequestration of pigments and antioxidant defences (Rennenberg, 1982; Alscher, 1989; Marrs, 1996; Coleman *et al.*, 1997a; May *et al.*, 1998; Noctor & Foyer, 1998; Noctor *et al.*, 1998). Levels of GSH alter in response to different types of biotic and abiotic stresses and it has been suggested that GSH may act both as a sensor for stress and as part of a very compact signal transduction system affecting the developmental plasticity of the root (Sánchez-Fernández *et al.*, 1997; May *et al.*, 1998; Reicheld *et al.*, 1999). To test this hypothesis, it is necessary to have reliable tools to quantify GSH levels in the appropriate tissue context. A range of sensitive biochemical assays have been developed for GSH in both its oxidized and reduced form (Anderson, 1985; Strohm *et al.*, 1995; Hermsen *et al.*, 1997); however, many of the key developmental events take place within a very limited number of cells in the meristem that cannot be purified for conventional biochemical analysis. We have adopted an alternative approach to measure GSH levels after enzyme-catalysed and therefore selective conjugation to monochlorobimane (MCB) in intact cells to give fluorescent glutathione S-bimane (GSB) (Kosower *et al.*, 1979; Newton & Fahey, 1995; Coleman *et al.*, 1997b; A. J. Meyer and M. D. Fricker, unpublished) that can be quantified by non-destructive confocal optical sectioning (Fricker *et al.*, 1997, 1998). Using this technique we previously reported that differences exist in the level of GSB fluorescence between different cell

types in the meristem, notably cells in the quiescent centre and the adjacent rapidly dividing initials (Sánchez-Fernández *et al.*, 1997). Although this approach provides comparative measurements of the average level of GSB fluorescence over the whole cell, conversion of the relative fluorescence intensities to concentrations of GSH in the cytoplasm requires correction for attenuation of the signal with increasing depth into the tissue (White *et al.*, 1996) and a method to compensate for the different levels of cytoplasm present in each cell type (Fricker *et al.*, 1998). We have previously developed empirical approaches to correct for the attenuation in fluorescence signal with increasing depth into biological specimens based on imaging a fixed and permeabilized specimen after infiltration with a reference dye (White *et al.*, 1996; Errington *et al.*, 1997; Fricker *et al.*, 1997, 1998). In this paper we have extended these empirical approaches to attenuation correction in *Arabidopsis* roots. In roots, the attenuation profile varies with distance from the meristem as the root anatomy and cell ultrastructure alters during cell division, elongation and differentiation. To account for the varying levels of cytoplasm, we have mapped the relative levels of protein in each cell type with distance from the meristem and used these values to determine the ratio of GSH level to protein content.

Materials and methods

Plant material

Seeds of *Arabidopsis thaliana* ecotype Col-0 were germinated on vertical agarose plates for 5–7 days at 21 °C under a 16 h light/8 h dark regime, as described previously (Sánchez-Fernández *et al.*, 1997).

Fluorescent dyes

Stocks of MCB (100 mM in ethanol), monobromobimane (MBB; 100 mM in ethanol), 5(− 6) carboxyfluorescein (CF; 53 mM in H_2O) and fluorescein isothiocyanate (FITC; 50 mM in H_2O) were stored at − 70 °C in 10 μL aliquots. Aliquots were thawed and diluted immediately prior to use. All dyes were obtained from Molecular Probes (Eugene, OR, U.S.A.).

Confocal imaging of glutathione S-bimane fluorescence

Intact seedlings of 5–7-day-old plants were transferred from agarose plates to a drop of 20–100 μM MCB on a coverslip and the root mounted in a slide–coverslip sandwich, separated by additional coverslips to provide a chamber approximately 170 μm deep. The open ends of the chamber were sealed with a thin track of grease to help immobilize the seedling and reduce evaporation. The cotyledons remained exposed to air throughout the measurement. The assembled chamber was positioned on the stage of a Nikon Diaphot inverted microscope. Room temperature was maintained between 18 °C and 20 °C. In some experiments, propidium iodide (PI) was added simultaneously with MCB to a final concentration of 10–50 μM.

Roots were imaged using a modified Bio-Rad MRC600 confocal laser scanning microscope (Fricker & White, 1992; Fricker *et al.*, 1994). The GSB conjugate was excited at 442 nm by a HeCd laser (Liconix, Santa Clara, CA, U.S.A.) equipped with neutral density filters to give an approximate power of 70 μW at the sample. The fluorescence emission for GSB was collected at 520 ± 45 nm using a Zeiss 25× 0.8 NA multi-immersion Neofluar lens or a Nikon 60× 1.4 NA PlanApochromat oil-immersion lens. In dual-labelling experiments with PI, the GSB signal was collected at 520 ± 45 nm and the PI signal at > 600 nm with a 565 nm dichroic mirror.

To follow the labelling kinetics, optical (x, y) sections were collected at the mid-plane of the root as a Kalman average of four frames and sampling repeated at 20–30 s intervals for 20–60 min. Data collection was typically started 3–5 min after exposure to MCB as the time required to assemble the chamber and position the root. Slight focus adjustments were often required to accommodate movement of the root as it grew.

To quantify the levels of GSB fluorescence, serial optical sections were collected with a mechanical focus increment of 1–3 μm over the complete depth of the root (typically 100 μm). Each optical section was Kalman averaged over 2–4 frames. Images were corrected for axial geometric distortion according to protocols described previously (White *et al.*, 1996; Errington *et al.*, 1997). The signal, after background subtraction, was assumed to be due entirely to fluorescence from the GSB conjugate, as there was no detectable auto-fluorescence under these imaging conditions. The intensity was calibrated against varying concentrations of GSB standards imaged under the same conditions as the roots.

After levels of GSB fluorescence were imaged, roots were fixed and then labelled with 50 μM FITC in phosphate buffered saline (PBS) for 30 min followed by three washes in PBS, to show the distribution of protein. Images were collected with the same instrument settings used for imaging GSB in roots. Protein images were also corrected for optical- and sample-dependent attenuation (see below).

Compensation for signal attenuation with increasing depth into the root

A model describing the attenuation of fluorescence by the sample was empirically determined from the loss of signal with depth in fixed and permeabilized roots infused with a 'sea' of carboxyfluorescein to try and achieve a uniform

distribution of fluorochrome predominantly in the vacuolar regions of the cells (White *et al.*, 1996; Fricker *et al.*, 1998). Roots were fixed and permeabilized according to Bauwens *et al.* (1994) and infused overnight with 53 μM CF in buffer (100 mM KCl, 10 mM NaCl, 1 mM $MgSO_4$, 25% EtOH, 10 mM 2-[N-morpholino]ethanesulfonic acid (MES) and 10 mM N-[2-hydroxyethyl]piperazine-N′-[2-ethanesulphonic] acid (HEPES), adjusted to pH 7.0 with Tris base). Fixed and permeabilized roots were mounted in the medium containing fluorochrome and serial optical sections collected with excitation at 442 nm with a z-motor step increment of 3 μm using the same instrument settings as used for imaging GSB. Several overlapping 3-D images were collected to span roughly 1 mm along the root. The 3-D (*x*, *y*, *z*) images were transposed into (x, y, z) images using the corrected *z*-sampling increment (i.e. a factor of 0.88, see White *et al.*, 1996). Each (*x*, *z*) section was then manually aligned on the centre of the root and sections averaged in 10–30 μm blocks along the length of the root, starting at the tip (Fig. 1a, c). Average fluorescence intensities were measured around the periphery of the root in each averaged block. In addition, the change in fluorescence with depth for the CF-medium was determined throughout the field and used as a shading corrector. To provide a more convenient parametric description of the fluorescence attenuation, a series of quadratic trendlines were fitted to the normalized intensities measured along the root at varying depths from the surface (Fig. 1e). The resulting family of curves describe the relative attenuation along the length, *l*, of the root with depth, *d*. The change in intensity was well described by a series of quadratic trendlines (Fig. 1e). Although these equations could be used to predict the level of attenuation with position in the root, a more compact description was obtained by modelling how the equations of the curves themselves altered with increasing depth. Thus, the coefficients for the 1st and 2nd order terms and the constant term from these trendlines were plotted vs. depth into the root (Fig. 1f–h) and each fitted with a 5th order polynomial describing how the coefficients varied with depth.

2nd order coefficient (*a*)

$$-2.30 \times 10^{-15}d^5 + 4.428 \times 10^{-13}d^4 - 2.065 \times 10^{-11}d^3 - 2.190 \times 10^{-11}d^2 - 3.467 \times 10^{-9}d + 3.372 \times 10^{-8} \quad (1)$$

1st order coefficient (*b*)

$$2.506 \times 10^{-12}d^5 - 4.651 \times 10^{-10}d^4 + 1.683 \times 10^{-8}d^3 + 5.296 \times 10^{-7}d^2 - 4.591 \times 10^{-6}d + 8.523 \times 10^{-6} \quad (2)$$

Constant term (*c*)

$$-8.627 \times 10^{-10}d^5 + 1.860 \times 10^{-7}d^4 - 1.041 \times 10^{-5}d^3 - 2.947 \times 10^{-5}d^2 - 1.378 \times 10^{-3}d + 1.004 \quad (3)$$

Equations (1)–(3) represent a compact form of the fluorescence attenuation for fixed and permeabilized roots in the form $attenuation = al^2 + bl + c$ and were used to calculate the attenuation at any depth along the root (Fig. 1i). The corresponding attenuation correction factors were subsequently derived as the inverse of the attenuation value expanded from this model for any given point along the root. To visualize the results of the attenuation correction, original or block-averaged 3-D images were adjusted by multiplication of each (*x*, *z*) section with an image calculated from the model (Fig. 1b, d).

Measurement of glutathione levels

To measure the average GSH level per cell, the average intensities for different regions were measured for each of five separate roots from mid-plane (*x*, *y*) images and each region corrected for attenuation using the corresponding

Fig. 1. Modelling the attenuation of fluorescence with depth into *Arabidopsis* roots. Panels (a) and (c) show optical (*x*, *z*) sections through an *Arabidopsis* root near the tip (a) and in the elongation zone (c) after fixation, permeabilization and infiltration with 5-CF. Few details of the root architecture can be distinguished after this treatment; however, the progressive loss in signal with depth through the root from the surface (uppermost) is readily apparent. The position of the root boundary is indicated in green. Panels (b) and (d) show optical (*x*, *z*) sections of an *Arabidopsis* root after labelling GSH with MCB. In the uncorrected images on the left-hand side, fluorescence is visible in all the cell layers of the root, but rapidly falls off with depth. The right half of each image shows partial restoration of the signal intensity using appropriate correction factors derived from the attenuation model presented in panels (e)–(i). Scale bar = 25 μm. Panel (e) represents the change in intensity within the epidermal cell layer along the CF-infiltrated root at nine different depths. Each curve was fitted with a 2nd order polynomial of the form $al^2 + bl + c$, where *l* is the length along the root from the tip. Panels (f)–(g) represent how the two coefficients (*a* = squared, *b* = linear) and the constant term (*c*) changed with increasing depth into the root. Each of these curves was fitted with a 5th order polynomial to provide three equations that described the level of attenuation for any depth or position along the root. The equations are given in the text. Panel (i) shows a 2-D surface plot expanded from these three equations. The fall-off in signal was sigmoidal and most pronounced in the denser tissues near the root apex. The attenuation gradually decreased on passing through the elongation zone around 400 μm from the tip to the region of root-hair initiation around 800 μm from the tip.

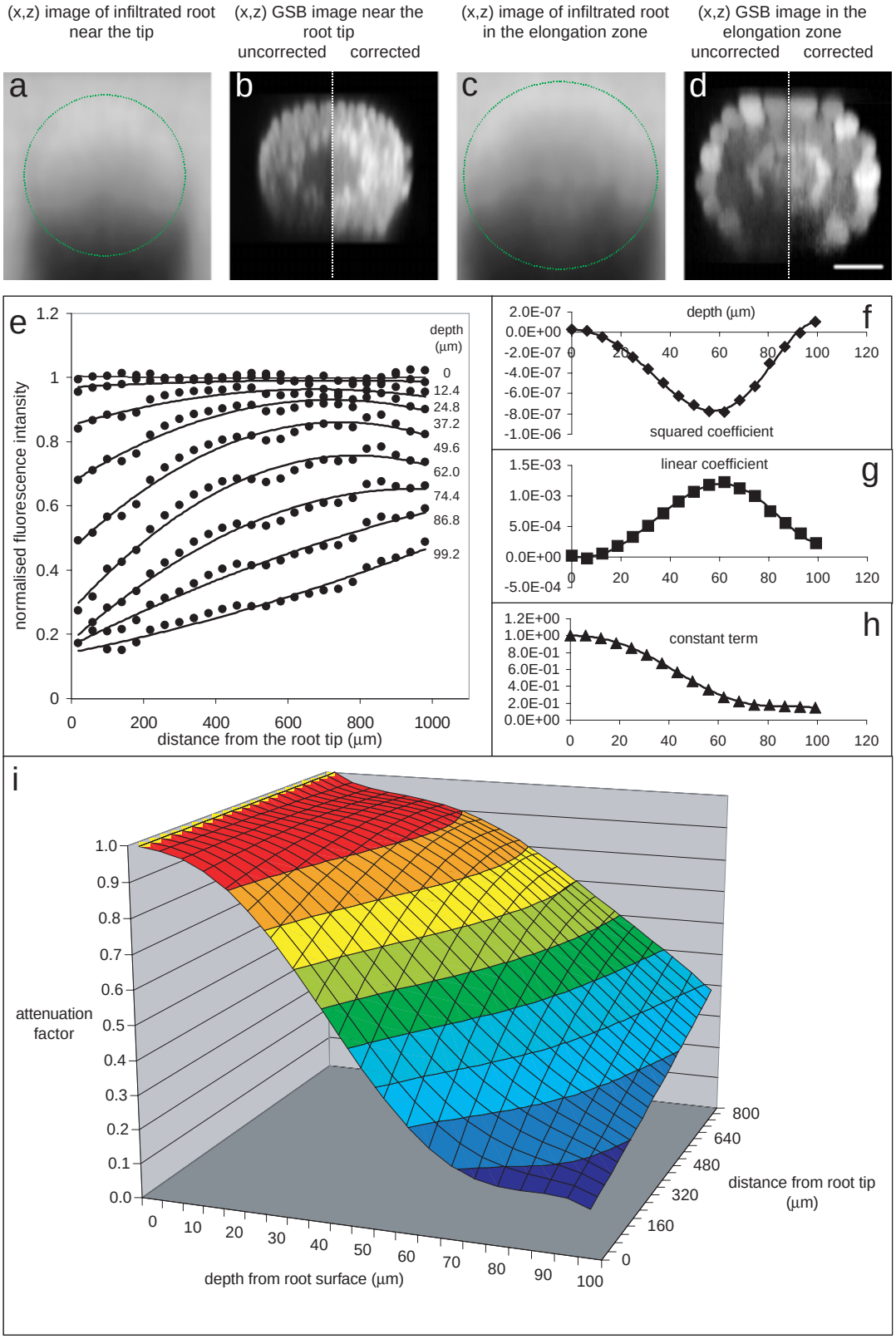
(x,z) image of infiltrated root near the tip
(x,z) GSB image near the root tip
uncorrected
corrected
(x,z) image of infiltrated root in the elongation zone
(x,z) GSB image in the elongation zone
uncorrected
corrected
a
b
c
d
e
normalised fluorescence intansity
distance from the root tip (µm)
depth (µm)
0
12.4
24.8
37.2
49.6
62.0
74.4
86.8
99.2
f
depth (µm)
squared coefficient
g
linear coefficient
h
constant term
i
attenuation factor
depth from root surface (µm)
distance from root tip (µm)

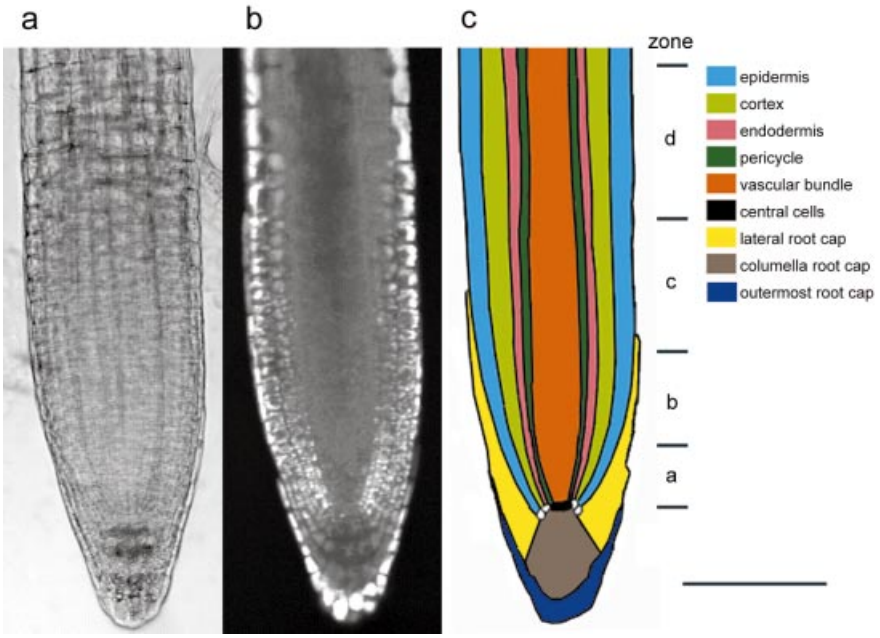

Fig. 2. Patterns of glutathione labelling in intact *Arabidopsis* roots. Panel (a) shows a non-confocal bright field image of a growing *Arabidopsis* root. The labelling pattern after 30 min in 100 μM MCB is shown for a single optical section in the mid-plane of the root in panel (b). A schematic representation of the various tissue layers is depicted in panel (c), along with the position of the arbitrary boundaries used to define zones for further analysis. Scale bar = 100 μm.

factor derived from the model. Corrected intensities were converted to average cellular GSH levels using the *in vitro* GSB calibration. Each value was also normalized for the average level of protein measured from a corresponding region of the fixed, permeabilized and FITC-labelled roots.

Software

Image processing and analysis were performed with the software packages COMOS™ and MPL™ (Bio-Rad Microsciences Ltd, Hemel Hempstead, U.K.), Scion Image™ (Scion Corporation, MD, U.S.A.) and Confocal Assistant™ (T.C. Brelje, University of Minnesota, U.S.A.). Images were assembled into montages using Photoshop™ (Adobe Systems Inc.). Graphical analysis of data from MPL was performed with Excel™ (Microsoft Corp.).

Results

Cells in the Arabidopsis *root are rapidly labelled with monochlorobimane*

Fluorescence increased rapidly in all cells examined in the *Arabidopsis* root in the presence of MCB and labelling resulted in a distinctive pattern in different cell types (e.g. Fig. 2b). There was essentially no autofluorescence under the imaging conditions used (data not shown). Labelling was specific for GSH as it was abolished completely in roots treated for 12 h with 1 mM buthionine sulphoximine (BSO), a specific inhibitor of γ-glutamyl-cysteine synthetase (γ-ECS), the first dedicated enzyme in the GSH synthesis pathway (data not shown). To determine the labelling kinetics for different cell types in the root, the change in average GSB fluorescence was followed in user-defined regions according to the template depicted in Fig. 2(c). The fluorescence intensity increased to a plateau in most cell types after about 15–20 min (Fig. 3a–c). It appears that MCB could rapidly diffuse to all cell layers in the root as there was no obvious lag period before development of fluorescence between different tissues, although it was not possible to record time-points earlier than about 3–5 min in this study due to the time required to assemble the root in the chamber on the stage. In some cell types, most notably the columella of the root cap and the developing vascular tissue within the stele, the fluorescence level declined after reaching the plateau value (Fig. 3a, b). Conversely, in the outermost cells of the root cap a gradual increase in fluorescence was observed that continued after fluorescence in most other cell types had reached a plateau (Fig. 3a). At the root tip, the rapidly dividing initials had a greater average fluorescence, roughly 25% higher than the central cells. Progressing away from this zone, several general trends were observed. First, the average fluorescence was greatest in the epidermal cell layer and decreased radially into the centre of the root. Second, it was not possible to clearly separate the signal from the endodermal layer and the pericycle or from tissues within the developing vascular tissue, so cells in these regions were grouped together. Third, the average fluorescence within each cell type, apart from the cap cells, decreased with distance from the meristem as the signal was diluted by the increase in cell volume with cell expansion in the elongation zone. For comparison, the labelling kinetics for the different cell layers just behind the meristem (zone b) and in the middle of the

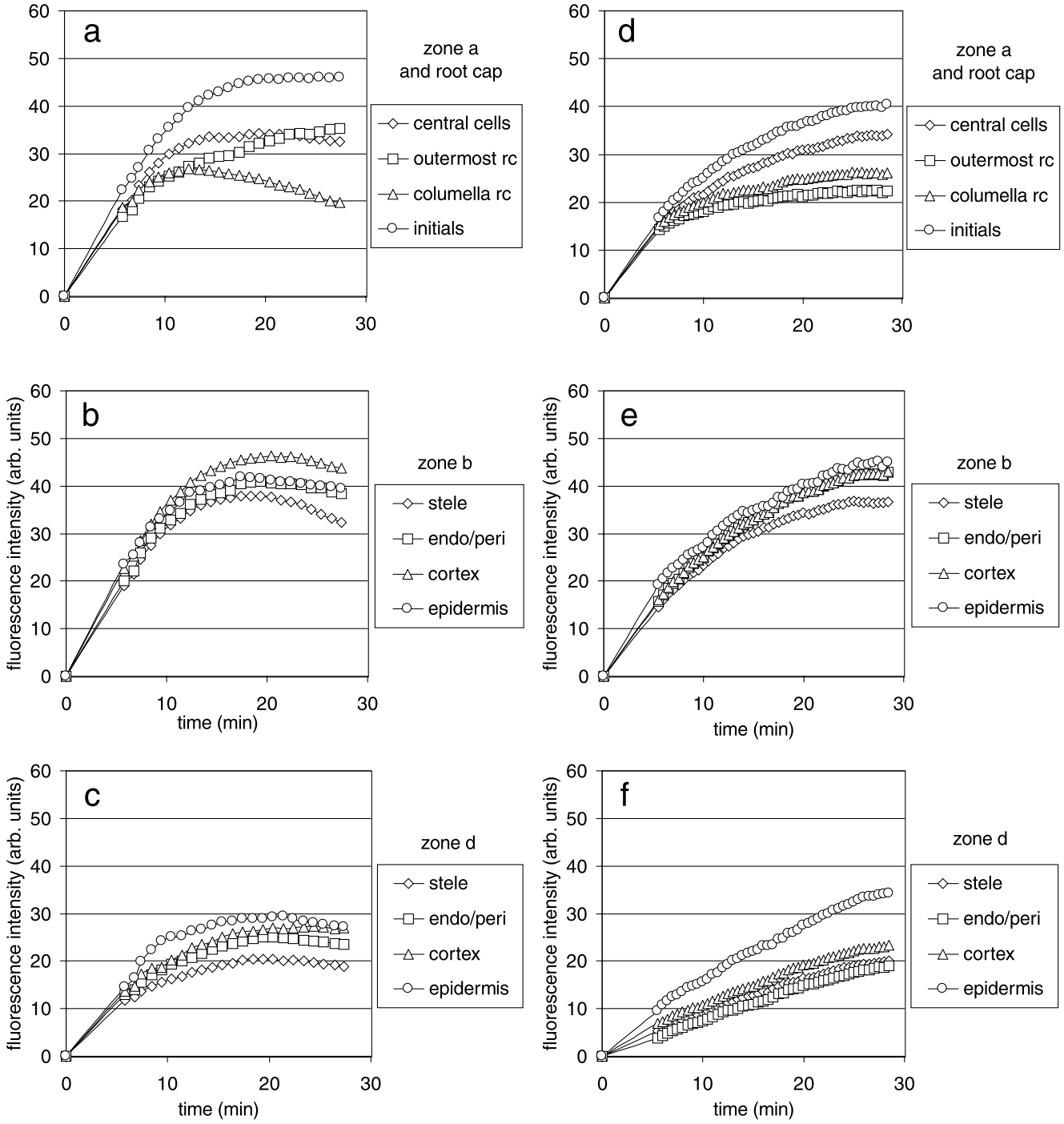

Fig. 3. Labelling kinetics for GSH for different cell types in intact roots of *Arabidopsis* in the absence and presence of azide. The average fluorescence intensity was measured with time for 16 different regions of the root after labelling with 100 μM MCB in the absence (a)–(c) or presence (d)–(f) of 1 mM sodium azide. Each trace represents the average of four (a)–(c) or three (d)–(f) roots for regions in zone a (a, d), zone b (b, e) and d (c, f), defined using the template shown in Fig. 2. It was not possible to clearly separate the endodermal and pericycle cell layers or the different cell types within the stele so data from these regions represent an average of more than one cell type. Single optical sections in the mid-plane of the root were averaged over four frames and sampling repeated at 20–30 s intervals with excitation at 442 nm using a 25× 0.8 NA lens. The delay between the start of labelling ($t = 0$) and the first data point represents the time required to align and focus the sample.

elongation zone (zone d) are presented in Figs 3(b) and (c), respectively.

Pre-treatment with 1 mM sodium azide (10 min) did not significantly alter the total fluorescence at the plateau level, but the rate of labelling was slower (Fig. 3d–f). This was most significant in zone d, where it took about 50% longer to reach the plateau value of fluorescence. There was no indication of a delay in labelling between different cell layers in the presence of azide; however, changes in fluorescence once the plateau level was reached were abolished. Thus, unlike control roots, the fluorescence did not decrease in the columella or increase in the outermost root cap cells (Fig. 3d–f).

It was anticipated that azide treatment would deplete ATP levels and thereby inhibit the activity of putative glutathione S-conjugate (GS-X) pumps on the tonoplast that transport GSB into the vacuole. In time-course measurements using the 60× lens, GSB fluorescence was observed to increase initially in the cytoplasm and label was then transferred to the vacuole (Fig. 4a). There was no evidence for conjugation or accumulation in cytoplasmic organelles, which were sometimes observed to be negatively stained. The nucleus was slightly brighter (about 20%) than the cytoplasm; however, a rigorous quantitative comparison was not attempted in this study as the negatively stained organelles and adjacent thin strip of unlabelled cell wall make it difficult to segment out the cytosolic GSB fluorescence unequivocally. The vacuole was not fluorescent initially, but accumulated fluorescent GSB conjugate rapidly and cleared much of the signal from the nucleus and cytoplasm within 30 min (Fig. 4a). Incubation in 1 mM sodium azide did not affect the labelling in the cytoplasm but substantially reduced transfer of GSB to the vacuole (Fig. 4b).

Quantification of glutathione S-bimane fluorescence levels – correction for depth- and sample-dependent attenuation

It was apparent that the signal from any particular cell type decreased markedly when focusing deeper into the root. This can be most readily appreciated for the epidermal cells, for example, in (x, z) sections through the root (e.g. Fig. 1b, d). Although it was possible to make quantitative measurements from the epidermal cells adjacent to the coverslip where the contribution of depth- and sample-dependent

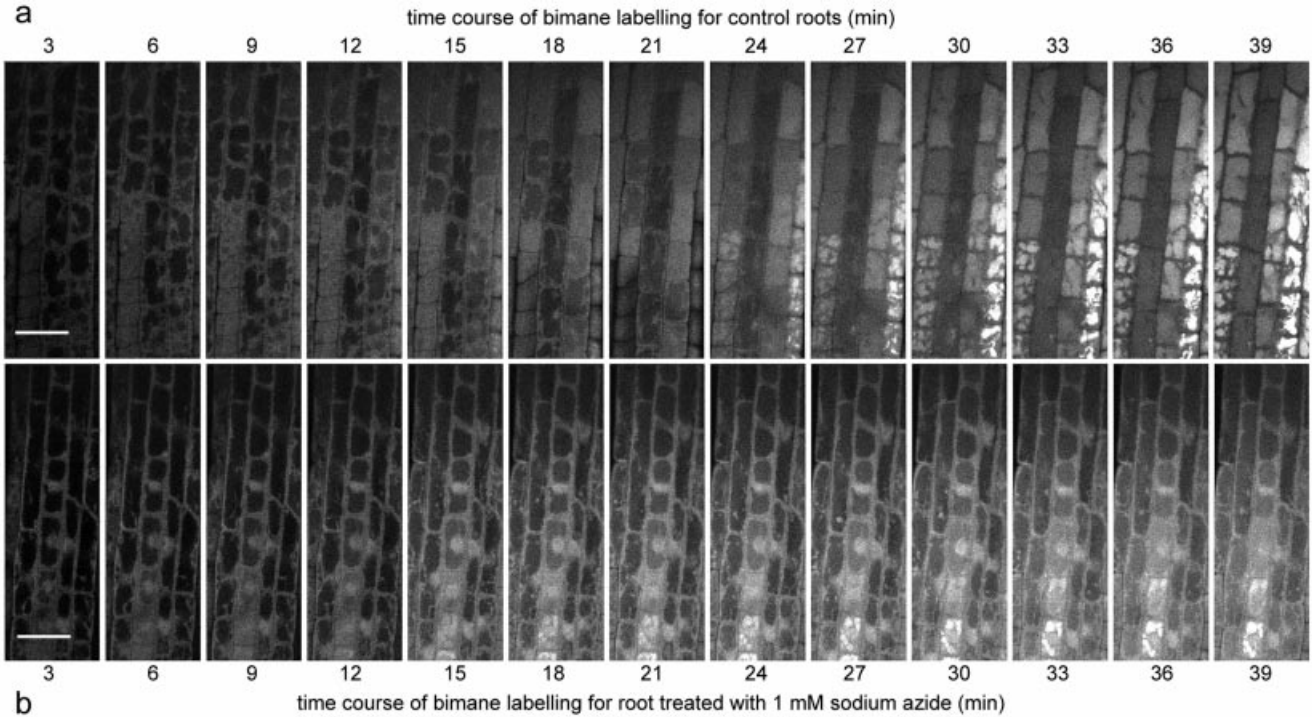

Fig. 4. Vacuolar sequestration of GSB in the absence and presence of azide. Panel (a) shows selected images from a time series to illustrate the increase in GSB labelling in the cytoplasm and its transfer into the vacuole over time. The time is given in minutes above each image. The trichoblast and atrichoblast cell files show different levels of fluorescence, with the trichoblasts being the brightest at the end of the experiment. The change in position of the cells reflects continued cell elongation during the course of the measurements. Panel (b) shows the effects of a 10 min pre-incubation in 1 mM sodium azide on the distribution of fluorescence. Although the total level of fluorescence increases to an amount comparable to the control root in panel (a), transfer of GSB to the vacuole is substantially inhibited. There is also very limited cell elongation under these conditions. Each sequence represents every 9th image from a time-series sampled at 20 s intervals from the epidermal cell layer with excitation at 442 nm using a 60× 1.4 NA lens. Scale bars = 25 μm.

attenuation were minimal, measurements from cells deeper into the tissue, such as the central cells, required compensation for the loss in signal. Furthermore, the extent of the fluorescence attenuation observed varied not only with depth but also along the length of the root. To obtain an estimate of the level of attenuation, a homogeneous reference distribution of fluorochrome was established within the tissues by fixing and permeabilizing roots and infiltrating them with carboxyfluorescein. Under these conditions, the decrease in fluorescence with depth was attributed primarily to the optical aberrations arising in microscope, immersion medium and specimen, and light scattering in the sample. A compact model was developed to describe the fluorescence attenuation with depth along the root (see Material and methods). The reciprocal of the model for a given depth and distance from the root tip provided attenuation correction factors that were partially effective in restoring fluorescence intensities at depths up to 50–70% of the depth of the root (Fig. 1b, d). The correction factor required at the mid-plane of the root varied from 1.1 to 1.8 for different cell types and regions of the root. Although the intensity value was increased after correction, the correction did not attempt to reduce the concomitant blurring observed with increasing depth. At depths much beyond the mid-plane the very low signal prevented useful measurements.

Virtually all the different cell types in the root meristem were visible in a single, longitudinal median optical section of the root (e.g. Fig. 2b). Correction of the signal attenuation using the model required knowledge about both the distance from the root tip and the depth into the root to derive the appropriate correction factor. To ensure that the GSH pool was fully labelled, 3-D images were collected after 20–30 min incubation in MCB. The average fluorescence intensity for defined cell types was measured for five roots according to the template shown (Fig. 2c). The average distance of each region from the root tip was measured from the same (x, y) image, whereas the distance from the root surface was measured from a corresponding (y, z) section of the original 3-D image after correction for axial distortion. These two parameters were used to calculate the attenuation correction factor for the region. The correction factors were used to restore the fluorescence intensities and the corrected values were converted to average cellular GSH levels with reference to GSB standards imaged using the same instrument settings (Fig. 5a). After this transformation, the highest GSH levels were found in the outermost cells of the root cap and the lowest within the vascular tissue.

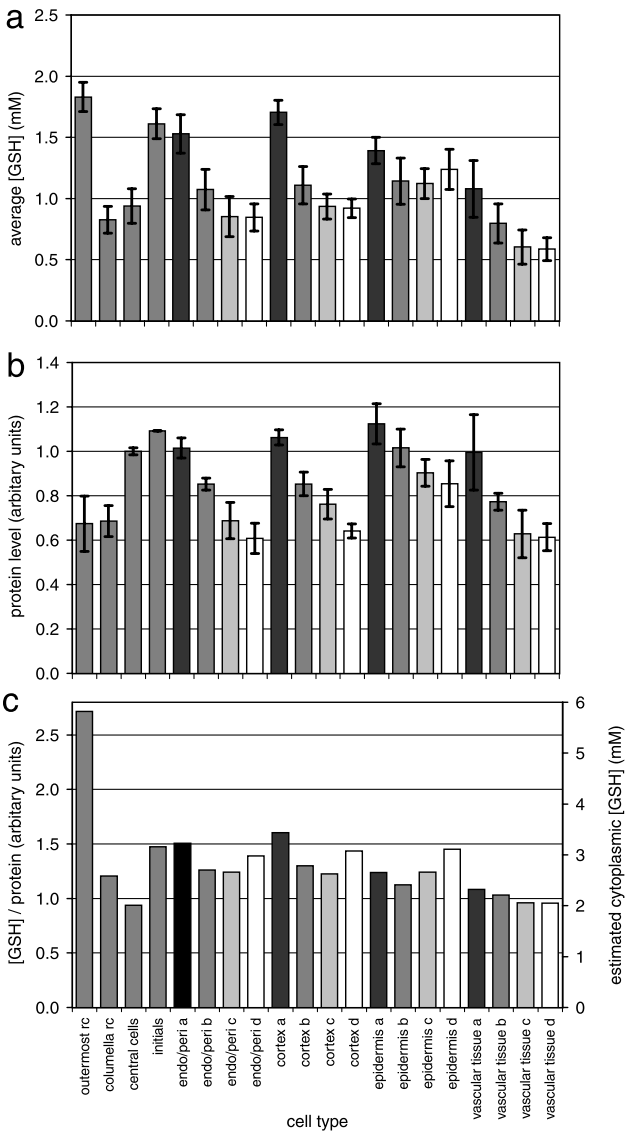

Fig. 5. Quantification of cellular GSH in intact *Arabidopsis* roots. Panel a shows the average concentration of GSH for particular cell types at varying distances from the root tip. Each value represents the mean of five experiments after background subtraction. Error bars are ± 1 SD. Panel (b) shows the level of protein for different cell types along the root, measured as the average fluorescence intensity following fixation, permeabilization and labelling with FITC. Each value represents the mean of five experiments after background subtraction and normalization to the intensity in the central cells. Error bars are ± SD. Panel (c) shows the ratio of GSH to protein calculated for each region from (a) and (b) and normalizes the average GSH concentration measured for changes in the volume of cytoplasm present in each region as the cells expand and differentiate. The right-hand axis gives the corresponding estimates of cytoplasmic glutathione concentration based on the ratio of protein to cytoplasmic volume measured for the epidermal cells in zone d. An average value of 40% cytoplasm was measured from manual segmentation of the cytoplasm and vacuole in serial optical sections of this region; all other regions are scaled in proportion to their protein content.

Normalization of glutathione levels for protein distribution

The absolute GSH level and the apparent decrease in each cell type with distance from the meristem were still misleading, however, as they represented the average GSH level for each cell and are weighted down by the increase in total cell volume with cell expansion. The amount of cytoplasm present in each cell type with increasing distance from the root tip was estimated from the level of FITC-protein fluorescence (Fig. 6c), normalized to the central cells (Fig. 5b). The average amount of protein was highest for cells within the meristematic region, with no significant differences between the rapidly dividing initials and the central cells, in contrast to the results following MCB labelling. The average protein level gradually declined on moving away from the meristem, but at slightly different rates for different cell types (Figs 5b, 6c), presumably following the respective differences in rates of cell division and enlargement. Normalization of the GSH level to protein level for each cell type (Fig. 5c) highlighted the high levels of GSH in the outermost cells of the root cap and also the marked difference between the central cells and the neighbouring initial cells. Ratioing against protein content reduced the apparent decline in GSH levels on moving away from the meristem for each cell type, with marginally higher levels near the meristem. There was relatively little difference in GSH levels between the epidermis, cortex and endodermal/pericycle cells on a protein basis; however, the vascular tissue apparently still maintains a lower GSH level.

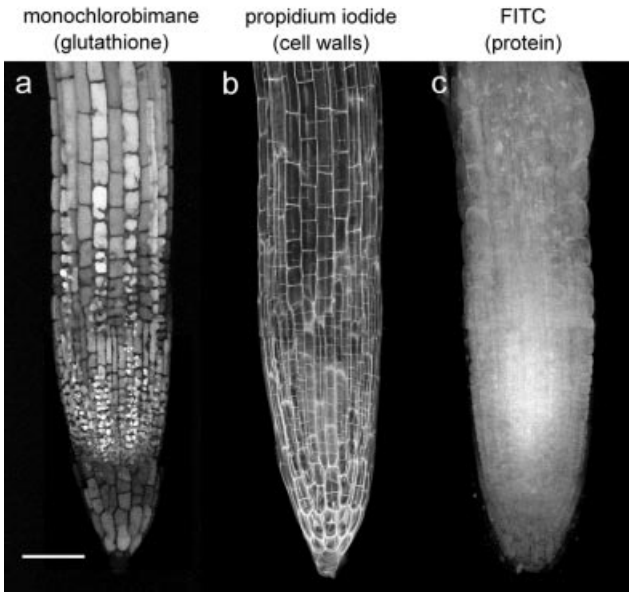

Fig. 6. Comparison between GSB fluorescence and protein labelling of an *Arabidopsis* root. Panel (a) is a maximum projection of an intact *Arabidopsis* root after 30 min labelling in 100 μM MCB. The GSB has been transported into the vacuole throughout the root and the characteristic pattern of trichoblast and atrichoblast labelling is apparent in the elongation zone. The bright cells towards the tip are the outermost cell layer of the lateral root cap. In this root, the columella and outermost layer of the root cap are relatively dim. Panel (b) is a maximum projection showing the cell walls labelled with propidium iodide and imaged simultaneously. No nuclei are labelled up, indicating that the root remained viable throughout the labelling and imaging procedure. In (c), the distribution of protein is shown as a maximum projection of the same root following fixation, permeabilization and labelling with FITC. The highest protein concentrations correspond to the meristematic zone of small, rapidly dividing cells. Fluorescence decreases on moving away from this region as the cells begin to elongate. Scale bar = 50 μm.

Estimation of cytoplasmic glutathione concentration

To express the average GSH levels measured in each region as the cytoplasmic glutathione concentration ($[GSH]_{cyt}$) required a conversion factor between the amount of protein measured by FITC labelling and the cytoplasmic volume. The amount of cytoplasm for epidermal cells in zone d was estimated as approximately 40% of the cell total by manually segmenting out the cytoplasm in 3-D images (data not shown). Using this estimate, the equivalent cytoplasmic volumes for different cell types and zones along the root were calculated in proportion to their corresponding protein measurements (presented on the right hand axis of Fig. 5c). Values for the outermost cells of the root cap were around 6 mM, the rapidly dividing initials were just over 3 mM, the central cells and vascular tissue were just below 2 mM and most other cell types were between 2 and 3 mM (Fig. 5c).

Discussion

Conjugation of GSH to bimanes *in situ* in plants is becoming an increasingly versatile technique to follow the pathway of GSH-mediated xenobiotic detoxification *in vivo* (e.g. Coleman *et al.*, 1997b), as a marker for vacuolar compartments (e.g. Swanson *et al.*, 1998) or as a prelude to subsequent analysis of cellular GSH levels via high-pressure liquid chromatography (HPLC) (Kosower *et al.*, 1979; Newton & Fahey, 1995; Strohm *et al.*, 1995). In this paper, we demonstrate that *in situ* labelling with MCB can be used to provide a quantitative measure of $[GSH]_{cyt}$ in every cell type of an intact root. The method relies on conjugation of MCB to GSH within the intact tissues to give a fluorescent GSB-conjugate that can be imaged using non-destructive confocal optical sectioning. Although in principle MCB can react with a wide range of low-molecular weight or protein thiol groups present within cells, the rate of non-enzymatic conjugation is very slow (Coleman *et al.*, 1997b; A. J. Meyer & M. D. Fricker, unpublished). Thus, specificity for GSH can be achieved by using relatively low concentrations of MCB (100 μM in this study) and

relying on GST-mediated conjugation to give both an adequate rate of reaction and specificity for GSH. We have shown previously (A. J. Meyer and M. D. Fricker, unpublished) that all the cytoplasmic GSH in *Arabidopsis* suspension culture cells is specifically labelled by MCB in an enzymatic reaction catalysed by a glutathione S-transferase(s). In this study we have not confirmed the specificity of the labelling for GSH in intact roots by HPLC, but we infer that the entire cytoplasmic GSH pool was conjugated in a GST-catalysed reaction as labelling reached a plateau in all cell types within about 20 min. For comparison, the time required to label the cytoplasmic GSH pool via a non-enzymatic second-order reaction at the temperature of the experiments (rate constant at 25 °C = 0.15 $\text{M}^{-1}\ \text{s}^{-1}$, A. J. Meyer and M. D. Fricker, unpublished observations) would be approximately 5000 min. In addition, there was no detectable protein thiol labelling by MCB under the conditions used, as all the GSB fluorescence was released from the root during the fixation and permeabilization steps used prior to protein labelling with FITC (data not shown). We also infer that MCB was able to penetrate rapidly into all cell layers at the root tip and did not significantly limit the rate of reaction, as there was no discernible lag period in the labelling kinetics for different cell types.

Quantitative measurements of the GSB fluorescence for each cell type require a method with sufficient spatial resolution to record the fluorescence intensities in intact, living roots. Confocal optical sectioning provides sufficient lateral and axial resolution to enable imaging within intact tissues. The shortest visible wavelength available in our multiple-laser confocal microscope (Fricker & White, 1992) is a 442 nm line from a HeCd laser, which gives about 20% excitation efficiency of GSB compared to the excitation maximum at 395 nm. Even at this low excitation efficiency, the relatively high levels of fluorescence achieved from labelling the entire GSH pool facilitated measurements at low laser power under conditions where roots continued to grow. Fortuitously, excitation at 442 nm also avoids photoactivation of fluorescence from non-conjugated MCB, sometimes observed with UV-excitation in conventional fluorescence microscopy as an increase in fluorescence in the medium (data not shown).

Although GSB fluorescence can clearly be imaged within the root, quantitative measurements are complicated by the loss in intensity with depth into the specimen. Partial correction for this signal attenuation was achieved by an empirical approach (White *et al.*, 1996; Errington *et al.*, 1997) based on measurement of the loss in signal with depth in a model system derived from the specimen after permeabilization and infiltration with a uniform 'sea' of carboxyfluorescein. The resultant axial intensity response combines the effects of depth-dependent 'sea' response and the additional contribution of the permeabilized tissue. Previously we have used a single attenuation function for sheets of epidermal tissue (White *et al.*, 1996) or cartilage explants (Errington *et al.*, 1997); however, in the *Arabidopsis* root the fluorescence attenuation varied along the length of the root as the root anatomy and cell density altered. We have therefore developed a 2-D correction function that varies both with depth into the tissue and length along the root. This was partially effective in restoring fluorescent intensities within the root. Without applying this correction, values would be underestimated by up to 50% for cells within the mid-section of the root. Strictly, the correction function was only derived for the epidermal tissue and may underestimate the extent of attenuation progressing radially into the centre of the root. This would then require a more complex correction procedure specifying depth, distance along the root and cell layer. We have not yet tested this possibility.

To translate the corrected GSH levels measured over a region of tissue to cytoplasmic GSH concentrations required measurement of the cytoplasm to total cell ratio for each cell type. A direct measure of the cytoplasmic volume is not straightforward at the light microscope level, but can be achieved from 3-D images of larger cell types, such as the epidermal cells, using manual segmentation or stereological techniques (Howard & Reed, 1998; Kubínová *et al.*, 1999; Meyer *et al.*, 2000). In this paper, we measured the percentage cytoplasm from 3-D images of epidermal cells in the elongation zone, which were sufficiently clear to allow manual segmentation of the cytoplasm. The level of cytoplasm for other cell types was estimated in proportion to their protein content.

Differences in estimated $[\text{GSH}]_{\text{cyt}}$ were observed between the central cells and the adjacent rapidly dividing initials, in line with our previous qualitative observations (Sánchez-Fernández *et al.*, 1997) and consistent with the view that the redox state of the cells is linked to the stage of the cell cycle (May *et al.*, 1998; Reicheld *et al.*, 1999). The estimated $[\text{GSH}]_{\text{cyt}}$ for most other cell types falls in the range 2–3 mM, with the notable exception of the outermost cells of the root cap. Comparison with values reported in other plant systems is difficult as most data are expressed in terms of nmol GSH per gram fresh weight and are averaged over a large bulk of tissue. We have not calculated the integral of the fluorescence measured in the root tip; however, assuming that the cytoplasm to total ratio is about 20% for the majority of cells in the root system and that cells have an average density of 1.02 g mL^{-1}, a $[\text{GSH}]_{\text{cyt}}$ of 2–3 mM measured in this study would correspond to around 390–590 nmol g^{-1} fresh wt. A lower estimate of the percentage cytoplasm would lower this estimate accordingly.

The GSB was also rapidly transferred to the vacuole in all cell types where vacuolar structures could be clearly resolved. We infer that *Arabidopsis* roots are well endowed with vacuolar GS-X pumps capable of transporting GSB (Martinoia *et al.*, 1993; Li *et al.*, 1995; Coleman *et al.*, 1997a, b; Ishikawa *et al.*, 1997; Rea *et al.*, 1998) that have

recently been cloned from *Arabidopsis* (Lu *et al.*, 1997, 1998; Tommasini *et al.*, 1997; Sánchez-Fernández *et al.*, 1998). The activity of these pumps appears to be particularly high in *Arabidopsis* roots. Lower rates of vacuolar sequestration were observed in other species such as tobacco (data not shown). Vacuolar sequestration is a normal part of the GSH-mediated detoxification pathway for xenobiotics (Coleman *et al.*, 1997a, b) and may precede degradation of the xenobiotic. Estimates of $[GSH]_{cyt}$ will be in error if the GSB is further metabolized to a point where the fluorescence is affected or re-mobilized out of the cell. In certain cell types, notably the columella and vascular tissue, the levels of fluorescence level declined after the plateau was reached. Several potential mechanisms may underlie these changes, including breakdown of the GSB (e.g. Wolf *et al.*, 1996), re-export from the cell across the plasma membrane or via cell–cell transport through plasmodesmata. As these changes were abolished by azide treatment, which also prevented transport of the GSB into the vacuole, it is tempting to speculate that the decreases reflect operation of a degradation pathway in the vacuole. Equally, however, it is intriguing to note that the increase in signal in the outermost cells of the root cap was also abolished in the presence of azide. It is possible that the sequestration component of the detoxification pathway is specifically enhanced in the outermost cells and that they act as a sink for GSB from other cells in the root cap that are symplastically connected. Given that these cells will shortly be sloughed off, this system might form a very efficient route to detoxify and effectively excrete xenobiotics from the root. These results also emphasize the important new insights that imaging techniques can bring to the study of metabolism at the cellular level in an intact system.

Acknowledgements

We would like to thank the following for financial support: INTAS (M.D.F. and M.M.); Nuffield Foundation (M.D.F.); Rhône-Poulenc Agriculture and the Bio Avenir Program (M.D.F., A.J.M., N.S.W.), Royal Society (M.D.F. and N.S.W.). N.S.W. is currently the Bio-Rad Fellow in Laser Scanning Microscopy in the Department of Plant Sciences, Oxford, U.K.

References

Alscher, R.J. (1989) Biosynthesis and antioxidant function of glutathione in plants. *Physiol. Plant.* **77,** 457–464.

Anderson, M.E. (1985) Determination of glutathione and glutathione disulphide in biological samples. *Meth. Enzymol.* **113,** 548–555.

Bauwens, S., Katsanis, K., Van Montagu, M., Van Oostveldt, P. & Engler, G. (1994) Procedure for whole mount fluorescence *in situ* hybridisation of interphase nuclei on *Arabidopsis thaliana*. *Plant J.* **6,** 123–131.

Coleman, J.O.D., Blake-Kalff, M.M.A. & Davies, T.G.E. (1997a) Detoxification of xenobiotics by plants: chemical modification and vacuolar compartmentation. *Trends Plant Sci.* **2,** 144–151.

Coleman, J.O.D., Randall, R. & Blake-Kalff, M.M.A. (1997b) Detoxification of xenobiotics in plant cells by glutathione conjugation and vacuolar compartmentation: a fluorescent assay using monochlorobimane. *Plant Cell Environ.* **20,** 449–460.

Errington, R.J., Fricker, M.D., Wood, J.L., Hall, A.C. & White, N.S. (1997) Four-dimensional imaging of living chondrocytes in cartilage using confocal microscopy: a pragmatic approach. *Am. J. Phys.* **272,** C1040–C1051.

Fricker, M.D., Chow, C.-M., Errington, R.J., May, M., Mellor, J., Meyer, A.J., Tlalka, M., Vaux, D.J., Wood, J. & White, N.S. (1997) Quantitative imaging of intact cells and tissues by multi-dimensional confocal microscopy. *Exp. Biol. Online*, **2,** 19. http://link.springer.de.

Fricker, M.D., Errington, R., Wood, J., Tlalka, M., May, M. & White, N.S. (1998) Quantitative confocal fluorescence measurements in living tissue. *Signal Transduction – Single Cell Techniques* (ed. by B. Van Duijn and A. Wiltink), pp. 409–441. Springer-Verlag, Berlin.

Fricker, M.D., Tlalka, M., Ermantraut, J., Obermeyer, G., Dewey, M., Gurr, S., Patrick, J. & White, N.S. (1994) Confocal fluorescence ratio imaging of ion activities in plant cells. *Scan. Microsc. Suppl.* **8,** 391–405.

Fricker, M.D. & White, N.S. (1992) Wavelength considerations in confocal microscopy of botanical specimens. *J. Microsc.* **166,** 29–42.

Hermsen, W.J.M., McMahon, P.J. & Anderson, J.W. (1997) Determination of glutathione in plant extracts as the 1-chloro-2,4-dinitrobenzene conjugate in the presence of glutathione S-transferase. *Plant Physiol. Biochem.* **35,** 491–496.

Howard, C.V. & Reed, M.G. (1998) *Unbiased Stereology. Three Dimensional Measurements in Microscopy.* Bios Scientific Publishers, Oxford.

Ishikawa, T., Li, Z.S., Lu, Y.P. & Rea, P.A. (1997) The GS-X pump in plant, yeast, and animal cells: structure, function and gene expression. *Biosci. Rep.* 17, 189–207.

Kosower, N.S., Kosower, E.M., Newton, G.L. & Ranney, H.M. (1979) Bimane fluorescent labels: labelling of normal human red cells under physiological conditions. *Proc. Natl. Acad. Sci. USA*, **76,** 3382–3386.

Kubínová, L., Janácek, J., Guiulak, F. & Opatrny, Z. (1999) Comparison of several digital and stereological methods for estimating surface area and volume of cells studied by confocal microscopy. *Cytometry*, **36,** 85–95.

Li, Z.-S., Zhao, Y. & Rea, P.A. (1995) Magnesium adenosine 5′-triphosphate energizes transport of glutathione-*S*-conjugates by plant vacuolar membrane vesicles. *Plant Physiol.* **107,** 1257–1268.

Lu, Y.-P., Li, Z.-S. & Rea, P.A. (1997) *AtMRP1* gene of *Arabidopsis* encodes a glutathione-*S*-conjugate pump: isolation and functional definition of a plant ABC transporter gene. *Proc. Natl. Acad. Sci. USA*, **94,** 8243–8248.

Lu, Y.P., Li, Z.-S., Drodowicz, Y.M., Hortensteiner, S., Martinoia, E.

& Rea, P.A. (1998) AtMRP2, an *Arabidopsis* ATP binding cassette transporter able to transport glutathione S-conjugates and chlorophyll catabolites: functional comparisons with AtMRP1. *Plant Cell*, **10,** 267–282.

Marrs, K.A. (1996) The functions and regulation of glutathione S-transferases in plants. *Ann. Rev. Plant Physiol. Plant Mol. Biol.* **47,** 127–158.

Martinoia, E., Grill, E., Tommasini, R., Kreuz, K. & Amrhein, N. (1993) ATP-dependent glutathione *S*-conjugate 'export' pump in the vacuolar membrane of plants. *Nature*, **364,** 247–249.

May, M.J., Vernoux, T., Leaver, C.J., Van Montagu, M. & Inzé, D. (1998) Glutathione homeostasis in plants: implications for environmental sensing and plant development. *J. Exp. Bot.* **49,** 649–667.

Meyer, A.J. & Fricker, M.D. (2000) Direct measurement of glutathione in epidermal cells of intact *Arabidopsis* roots by two-photon laser scanning microscopy. *J. Microsc.* **198,** 174–181.

Newton, G.L. & Fahey, R.C. (1995) Determination of biothiols by bromobimane labeling and high-performance liquid chromatography. *Meth. Enzymol.* **251,** 148–166.

Noctor, G., Arisi, A.-C.M., Jouanin, L., Kunert, K.J., Rennenberg, H. & Foyer, C.H. (1998) Glutathione: biosynthesis, metabolism and relationship to stress tolerance explored in transformed plants. *J. Exp. Bot.* **49,** 623–647.

Noctor, G. & Foyer, C.H. (1998) Ascorbate and glutathione: keeping active oxygen under control. *Ann. Rev. Plant Physiol. Plant Mol. Biol.* **49,** 249–279.

Rea, P.A., Li, Z.-S., Lu, Y.P., Drozdowicz, Y.M. & Martinoia, E. (1998) From vacuolar GS-X pumps to multispecific ABC transporters. *Ann. Rev. Plant Physiol. Plant Mol. Biol.* **49,** 727–760.

Reicheld, J.-P., Vernoux, T., Lardon, F., Van Montagu, M. & Inzé, D. (1999) Specific checkpoints regulate plant cell cycle progression in response to oxidative stress. *Plant J.* **17,** 647–656.

Rennenberg, H. (1982) Glutathione metabolism and possible biological roles in higher plants. *Phytochemistry* **21,** 2771–2781.

Sánchez-Fernández, R., ArdilesDiaz, W., Van Montagu, M., Inzé, D. & May, M.J. (1998) Cloning and expression analyses of AtMRP4, a novel MRP-like gene from *Arabidopsis thaliana*. *Mol. Gen. Genet.* **258,** 655–662.

Sánchez-Fernández, R., Fricker, M.D., Corben, L.B., White, N.S., Sheard, N., Leaver, C.J., Van Montagu, M., Inzé, D. & May, M.J. (1997) Cell proliferation and hair tip growth in the *Arabidopsis* root are under mechanistically different forms of redox control. *Proc. Natl. Acad. Sci. USA*, **94,** 2745–2750.

Strohm, M., Jouanin, L., Kunert, K.J., Pruvost, C., Polle, A., Foyer, C.H. & Rennenberg, H. (1995) Regulation of glutathione synthesis in leaves of transgenic poplar (*Populus tremula x P. alba*) overexpressing glutathione synthetase. *Plant J.* **7,** 141–145.

Swanson, S.J., Bethke, P. & Jones, R.L. (1998) Barley aleurone cells contain two types of vacuoles: characterisation of lytic organelles by use of fluorescent probes. *Plant Cell*, **10,** 685–698.

Tommasini, R., Vogt, E., Schmid, J., Fromentau, M., Amrhein, N. & Martinoia, E. (1997) Differential expression of genes coding for ABC transporters after treatment of *Arabidopsis thaliana* with xenobiotics. *FEBS Lett.* **411,** 206–210.

White, N.S., Errington, R.J., Fricker, M.D. & Wood, J.L. (1996) Aberration control in quantitative imaging of botanical specimens by multidimensional fluorescence microscopy. *J. Microsc.* **181,** 99–116.

Wolf, A.E., Dietz, K.J. & Schröder, P. (1996) A carboxypeptidase degrades glutathione conjugates in the vacuole of higher plants. *FEBS Lett.* **384,** 31–34.